Protein Cell, 2025, **16**, 799–814
https://doi.org/10.1093/procel/pwaf042
Advance access publication 10 June 2025
Research Article

Protein & Cell

Research Article

Spatiotemporal characterization of disease-associated neurons in the entorhinal cortex-hippocampal circuit during Alzheimer's disease progression

Yuting Ma[1,2,3,‡], Juan Zhang[4,5,6,7,‡], Hankui Liu[1,3,8,‡], Dingfeng Li[4,5,‡], Sicheng Guo[1,2,3,‡], Jialuo Han[4,5], Lei Wang[9], Shaojun Yu[9], Xi Su[1,3], Yongchang Gao[1,10], Xiumei Lin[9], Ciren Asan[1,3], Yushan Peng[9], Guibo Li[9], Hui Jiang[1,9], Wei Wang[1], Huanming Yang[11], Jian Wang[11], Shida Zhu[1], Lijian Zhao[1,3,8,12,13,*], Jianguo Zhang[1,3,8,13,*], Qiang Liu[4,5,6,7,*]

[1]BGI Genomics, Shenzhen 518083, China
[2]College of Life Sciences, University of Chinese Academy of Sciences, Beijing 100049, China
[3]Hebei Industrial Technology Research Institute of Genomics in Maternal & Child Health, Clin Lab, BGI Genomics, Shijiazhuang 050000, China
[4]Hefei National Research Center for Physical Sciences at the Microscale, Division of Life Sciences and Medicine, University of Science and Technology of China, Hefei 230027, China
[5]Anhui Province Key Laboratory of Biomedical Aging Research, University of Science and Technology of China, Hefei 230027, China
[6]CAS Key Laboratory of Brain Function and Disease, University of Science and Technology of China, Hefei 230026, China
[7]Center for Advanced Interdisciplinary Science and Biomedicine of IHM, Division of Life Sciences and Medicine, University of Science and Technology of China, Hefei 230071, China
[8]Hebei Provincial Technology Innovation Center for Precision Medicine Diagnosis and Quality Control, Shijiazhuang 050000, China
[9]BGI Research, Shenzhen 518083, China
[10]School of Artificial Intelligence, University of Chinese Academy of Sciences, Beijing 100049, China
[11]BGI, Shenzhen 518083, China
[12]Medical Technology College, Hebei Medical University, Shijiazhuang 050000, China
[13]School of Public Health, Hebei Medical University, Shijiazhuang 050000, China

[‡]Equal contribution.
[*]Correspondence: zhaolijian@bgi.com (L. Zhao), zhangjg@genomics.com (J. Zhang), liuq2012@ustc.edu.cn (Q. Liu)

Abstract

The entorhinal cortex (EC)-hippocampal (HPC) circuit is particularly vulnerable to Alzheimer's disease (AD) pathology, yet the underlying molecular mechanisms remain unclear. By employing the high-depth sequencing strategy Smart-seq2, we tracked gene expression changes across various neuron types within this circuit at different stages of AD pathology. We observed a decrease in the extent of gene expression changes in AD versus wild-type (WT) mice as the disease advanced. Functionally, we demonstrate that both mitochondrial and ribosomal pathways were increasingly activated, while neuronal pathways were inhibited with AD progression. Our findings indicate that the reduction of EC-stellate cells disrupts Meg3-mediated energy metabolism, contributing to energy dysfunction in AD. Additionally, we identified GFAP-positive neurons as a distinct population of disease-associated neurons, exhibiting a loss of neuronal-like characteristics, alongside the emergence of glia- and stem-like features. The number of GFAP-positive neurons increased with AD progression, a trend consistently observed in both AD model mice and AD patients. In summary, this study identifies and characterizes GFAP-positive neurons as a novel subtype of disease-associated neurons in AD pathology, providing insights into their potential role in disease progression.

Keywords Alzheimer's disease, EC-HPC neuronal circuit, Smart-seq2, GFAP, energy metabolism

Received 10 February 2025; **accepted** 15 April 2025.

Introduction

Alzheimer's disease (AD) is the most common neurodegenerative disease, characterized by amyloid plaque deposition, glial activation, and synaptic loss, which ultimately leads to memory impairment and behavioral disturbances (Holtzman et al., 2011). The entorhinal cortex (EC)-hippocampal (HPC) neuronal circuit plays a crucial role in learning, memory, and spatial navigation, and is among the most vulnerable brain regions during AD progression (Grøntvedt et al., 2018). Structural, functional, and metabolic abnormalities in the EC-HPC neuronal circuit have been shown to emerge before the clinical symptoms of AD (Braak and Braak, 1990; Grøntvedt et al., 2018; Igarashi, 2023; Jun et al., 2020; Kunz et al., 2015; Moser et al., 2015; Yao et al., 2021; Ying et al., 2022). Understanding the cellular and molecular changes in this circuit in response to AD pathologic abnormalities is essential for deepening our knowledge of AD progression and identifying potential biomarkers and therapeutic targets.

Single-cell analysis provides a high-resolution approach to studying cellular diversity in the brain during AD pathology (Chen et al., 2020; Habib et al., 2020; Kenigsbuch et al., 2022; Keren-Shaul et al., 2017; Leng et al., 2021; Mathys et al., 2019), offering insights into the cellular and molecular mechanisms underlying the disease. While most previous studies have utilized UMI-based single-cell sequencing technology, which enables higher cell throughput, but this approach has limited efficiency in capturing low-abundance transcripts. Additionally, these studies have typically focused on neuronal cells at a single time point, lacking comprehensive assessments across different brain regions and disease stages. Therefore, a more integrated study capturing the dynamic changes across multiple ages and regions is necessary to enhance our understanding of AD pathology.

APP/PS1 transgenic mice, a widely used model for AD research, express human amyloid precursor protein (APP) and a mutant human presenilin 1 (PS1), both linked to early-onset familial Alzheimer's disease. In these mice, amyloid plaques typically begin to appear in the brain around 6 months of age, with plaque deposition progressively increasing as they age (Arendash et al., 2001). In this study, we utilized APP/PS1 transgenic mice to investigate pathological changes in the EC-HPC circuit, encompassing the EC, hippocampal CA1, and CA3 regions. To explore the fine pathological alterations and molecular mechanisms of neurons in the EC-HPC circuit at different disease stages, we collected neurons at 6 (early stage), 9 (mid stage), and 12 (late stage) months of age to assess changes across different brain regions and stages of disease progression. Using Smart-seq2 technology for single-cell full-length transcriptome sequencing, we discovered that neurons in APP/PS1 mice exhibited more extensive gene expression changes compared with WT mice, with this difference diminishing as AD progressed. Pathway analysis revealed a significant activation of energy metabolism pathways alongside the inhibition of neuronal pathways as the disease advanced.

We observed a reduction in the number of EC-stellate neurons as AD progressed, which contributes to the observed energy dysfunction. Notably, we found that the non-coding RNA Meg3 emerged as a key regulator of energy metabolism. Additionally, we identified a subpopulation of *GFAP*-positive neurons, which we classify as a distinct type of disease-associated neurons. These neurons exhibited a loss of neuronal-like features and an emergence of both glial and stem-like characteristics. The number of *GFAP*-positive neurons increased significantly during AD progression, a trend consistently observed in both AD model mice and AD patients. Collectively, our findings characterize *GFAP*-positive neurons as disease-associated neurons in AD pathology, highlighting their potential as both diagnostic and therapeutic targets.

Results

In-depth single-cell interrogation of EC-HPC circuit neurons in WT and APP/PS1 transgenic mice at various ages

We selected neuronal nuclei from the EC, hippocampal CA1, and hippocampal CA3 regions of male APP/PS1 and WT mice at 6, 9, and 12 months of age (6M, 9M, and 12M). Using flow cytometry, we isolated these nuclei and performed single-nucleus RNA sequencing with Smart-seq2 (Fig. 1A). Smart-seq2 is a comprehensive sequencing method that provides full-length transcriptome sequencing, capturing both gene expression and transcript structure (Fig. 1A).

In total, we generated expression profiles for 1,710 single neuronal nuclei, resolving 1,663 nuclei after quality filtering. These included 567 nuclei from the EC, 568 nuclei from CA1, and 551 nuclei from CA3. On average, ~5,500 expressed genes per nucleus were detected (Fig. 1B). Quality control metrics indicated low mitochondrial contamination, with the average mitochondrial ratio below 0.25% (Fig. 1B).

To classify neurons across different genotypes, ages, and brain regions, we conducted unsupervised clustering. This analysis revealed two main categories: glutamatergic (91.52%, marked by *Slc17a7*) and GABAergic neurons (8.48%, marked by *Gad2*) (Fig. 1C and 1D). We further identified nine distinct neuronal clusters within the EC-HPC circuit using neuronal markers (Fig. 1C and 1D) (Bergmann et al., 2022; Rosenberg et al., 2018).

These clusters included: EC pyramidal neuron subset 1 (EC-Pyr 1) (23.87%, marked by *Mef2c*, *Cux2*, *Cux1*), EC pyramidal neuron subset 2 (EC-Pyr 2) (8.30%, marked by *Tbr1*, *Htr1f*, *Foxp2*, *Tle4*, *Grik3*), EC-stellate neurons

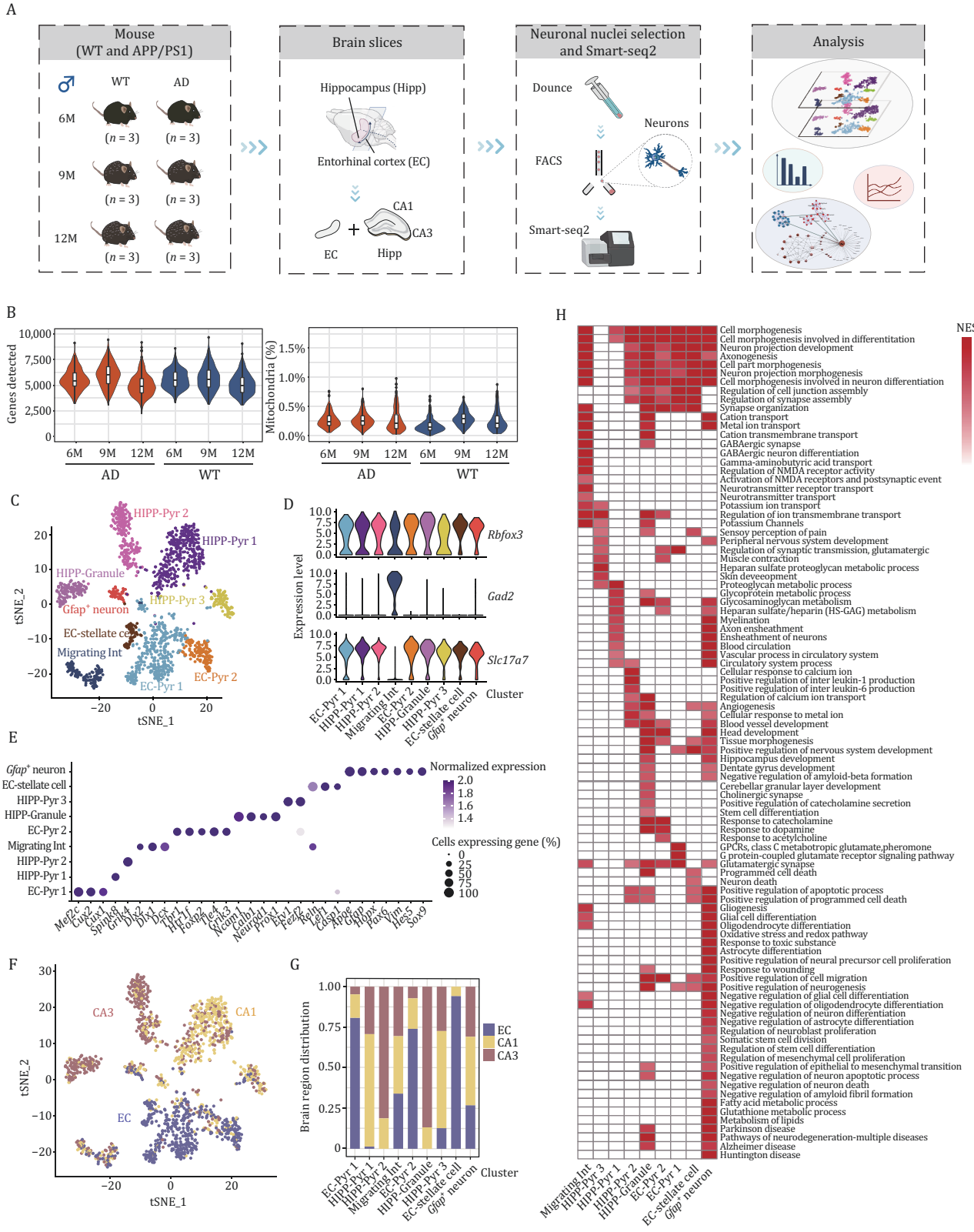

Figure 1. Characterization of neuronal diversity in the EC-HPC neural circuit. (A) Workflow of snRNA-seq. Neuronal nuclei were isolated from the EC-HPC circuit of APP/PS1 and WT mice at 6, 9, or 12 months of age, followed by to Smart-seq2 sequencing. (B) Average number of detected genes per nucleus and mitochondrion contamination levels. (C) t-SNE plot showing clustering of single neuronal nuclei. (D) Violin plots showing expression of marker genes: *Rbfox3* (pan-neuronal), *Gad2* (GABAergic neurons), and *Slc17a7* (glutamatergic neurons) across the clusters in (C). (E) Signature gene expression for each neuronal cluster. (F) t-SNE plot with nuclei colored by brain region. (G) Distribution of neuronal clusters within the indicated brain regions. (H) Pathway enrichment analysis for each neuronal cluster (significant threshold: $P < 0.01$, NES > 1.2).

(EC-stellate cell) (4.15%, marked by *Lef1*, *Reln*), hippocampal pyramidal neuron subset 1 (HIPP-Pyr 1) (23.57%, marked by *Spink8*), hippocampal pyramidal neuron subset 2 (HIPP-Pyr 2) (14.19%, marked by *Grik4*), hippocampal pyramidal neuron subset 3 (HIPP-Pyr 3) (6.13%, marked by *Fezf2*, *Etv1*), hippocampal granule neurons (HIPP-Granule) (8.18%, marked by *Prox1*, *Neurod1*, *Calb1*, *Ncam1*), migrating interneurons (Migrating Int) (8.48%, marked by the *Dlx1*, *Dlx2*, *Dcx*), and *Gfap*-expressing neurons (*Gfap*$^+$ neurons) (3.13%, marked by *Gfap*, *ApoE*, *Hopx*, *Pax6*, *Vim*, *Hes5*, *Sox9*) (Fig. 1C, 1E; Table S1). Interestingly, annotation of *Gfap*$^+$ neurons revealed that, in addition to NeuN, these cells expressed *Gfap*, *Aqp4*, and *Olig1* (glial markers), along with *Hopx*, *Sox9*, *Pax6*, *Vim*, and *Vcam1* (stem cell markers) (Fig. 1E). This suggests that *Gfap*$^+$ neurons exhibit both glial and stem-like characteristics.

When neurons were annotated by brain regions, we found that EC-Pyr 1, EC-Pyr 2, and EC-stellate cells were primarily localized in the EC, whereas HIPP-Pyr 1 and HIPP-Pyr 3 were mainly in the hippocampal CA1 region, HIPP-Pyr 2 and HIPP-Granule were primarily localized in the hippocampal CA3 region. Notably, both Migrating Int and *Gfap*$^+$ neurons were evenly distributed across the EC, hippocampal CA1, and hippocampal CA3 regions, as well as across different ages and genotypes (Figs. 1F, 1G and S1A).

To functionally characterize these neuronal clusters, we performed Gene Ontology (GO) enrichment analysis. We found that EC-Pyr 2, EC-Pyr 1, and EC-stellate cells were functionally related to "axonogenesis" and "neuron projection morphogenesis." EC-Pyr 2 neurons were linked to "response to catecholamine, dopamine, or acetylcholine," while EC-Pyr 1 neurons were related to "glutamatergic synapse," and EC-stellate neurons were related to "neuron death." Migrating Int neurons were linked to "GABAergic synapse," HIPP-Granule neurons to "hippocampus development" and "tissue morphogenesis," HIPP-Pyr 1 neurons to "myelination," HIPP-Pyr 2 neurons to "interleukin production," and HIPP-Pyr 3 neurons to "ion transport" and "peripheral nerve" (Fig. 1H; Table S2).

Notably, *Gfap*$^+$ neurons were functionally related to neural precursor cell proliferation, astrocyte and oligodendrocyte differentiation, and genesis, highlighting their distinct role in AD progression. Additionally, both HIPP-Granule and *Gfap*$^+$ neurons were functionally linked to amyloid β (Aβ) metabolism, suggesting that these two subtypes contribute to AD pathology by modulating Aβ metabolism.

Analysis of spatiotemporal differences and identification of disease-associated neurons in EC-HPC neural circuits

We next compared differential gene expression patterns in neurons isolated from the EC, CA1, and CA3 regions of APP/PS1 and WT mice at various ages. We found that the number of differentially expressed genes (DEGs) in APP/PS1 mice compared with WT mice at 6M (early AD progression) was significantly higher than at 9M (middle stage of AD) and 12M (late stage of AD) (Fig. 2A).

At 6M, the number of DEGs in EC neurons was notably greater than in hippocampal neurons in APP/PS1 compared with WT mice (Fig. 2A). The number of DEGs in both EC and hippocampal neurons decreased substantially from 6M to 9M in APP/PS1 versus WT mice (Fig. 2A; Table S3). Interestingly, while the number of DEGs in EC neurons continued to decline from 9M to 12M in APP/PS1 mice, the number of DEGs in hippocampal CA1 and CA3 neurons increased from 9M to 12M in APP/PS1 mice, compared with WT mice (Fig. 2A; Table S3). The overlap of DEGs across different brain regions and ages were surprisingly limited (Fig. 2B), indicating a strong spatiotemporal specificity in gene expression during AD progression. Moreover, neurons in the "EC-stellate" and "*Gfap*$^+$ neurons" clusters exhibited a significantly higher number of DEGs compared with neurons in other clusters in APP/PS1 versus WT brains (Fig. 2C; Table S4). This finding suggests that neurons in these two clusters play a major role in AD pathology, identifying them as disease-associated neurons.

Gene Set Enrichment Analysis (GSEA) revealed that most pathways were inhibited at 6M and 9M but became activated by 12M in APP/PS1 mice compared with WT mice (Figs. 2D and S1B; Table S5). Specifically, pathways related to mitochondrial respiratory function, superoxide generation, and ribosome function transitioned from repression to activation as AD pathology progressed (Fig. 2D). Conversely, pathways associated with neuronal functions, such as "synaptic membrane," "synaptic assembly," and "synaptic vesicle extracellular secretion," showed continuous reduction from 6M to 9M and 12M, with an exception of the EC at 9M. Additionally, pathways involved in β-amyloid formation and clearance were activated in CA3 as early as 9M in APP/PS1 mice, whereas similar activation in CA1 and EC occurred at 12M (Fig. 2D). Neuroinflammation, which often affects vulnerable regions in the AD brain, was also observed as well. We found that pathways related to inflammation, such as interleukin production, were activated in the EC and CA3 of APP/PS1 mice as early as 6M. In contrast, pathways related to other cytokine production were activated in CA1 of APP/PS1 mice at a later stage (9M) (Fig. 2D; Table S5). The extent of these changes was notably greater in hippocampal CA3 than in EC and CA1 of APP/PS1 mice (Fig. 2D).

We next conducted pathway analysis for EC-stellate and *Gfap*$^+$ neurons, which displayed substantial changes in gene expression patterns in APP/PS1 versus WT brains compared with neurons in other clusters (Fig. 2E and 2F). We found that mitochondrial respiratory function in EC-stellate neurons—a type of neuron highly dependent on energy and crucial for spatial memory (Crotty et al.,

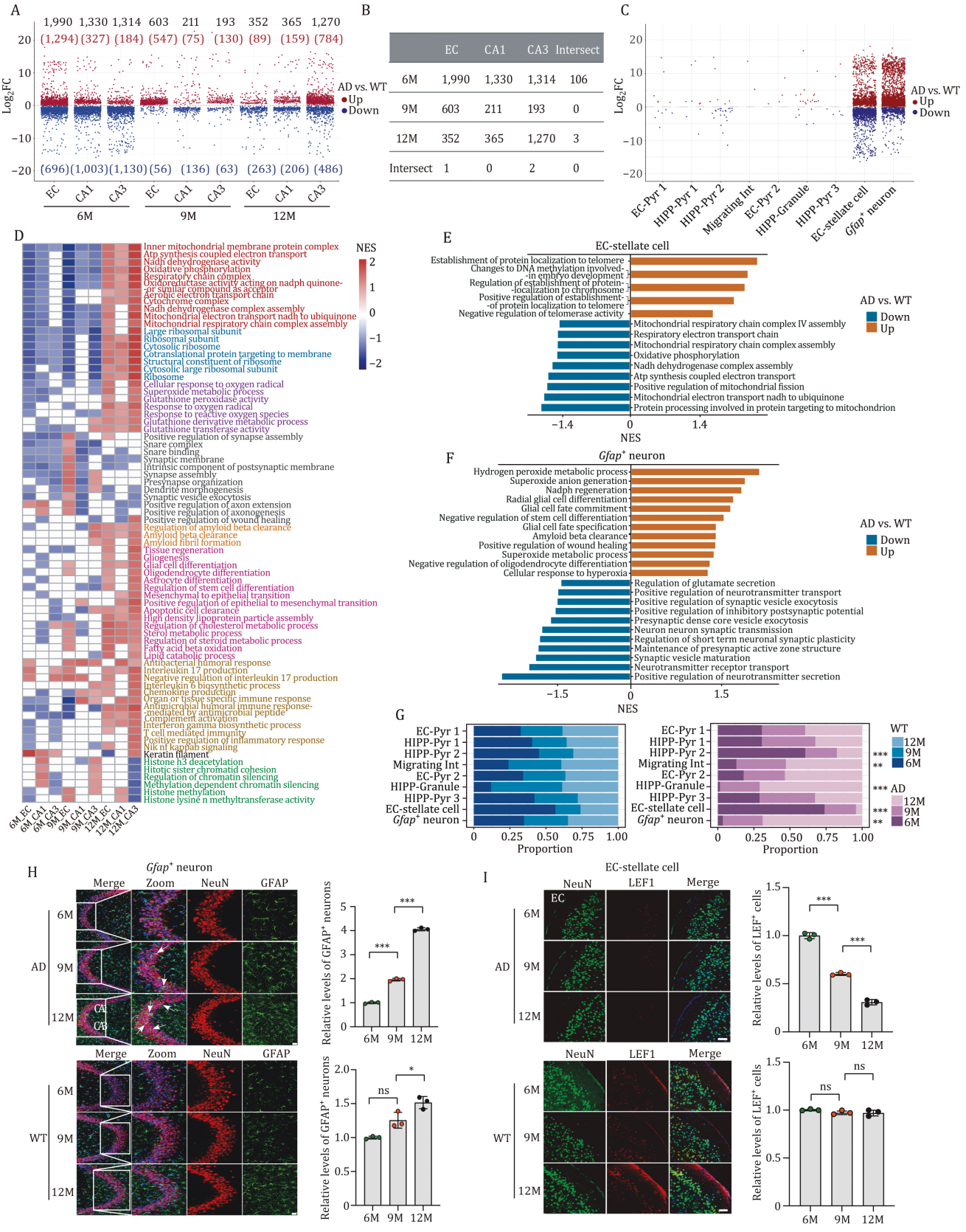

Figure 2. EC-stellate and GFAP⁺ neurons show distinct molecular features during AD progression. (A) Differentially expressed genes (DEGs) in neurons isolated from the EC, CA1, and CA3 regions of APP/PS1 and WT mice at 6, 9, and 12 months of age. (B) Number of DEGs across the indicated brain regions and ages in APP/PS1 versus WT mice. (C) DEGs identified in each neuronal cluster between APP/PS1 and WT mice. (D) Gene Set Enrichment Analysis (GSEA) comparing AD and WT mice at the indicated ages and brain regions. (E) GSEA of EC-stellate cells in AD versus WT mice. (F) GSEA of *Gfap*⁺ neurons in AD versus WT mice. (G) Distribution of neuronal numbers in each cluster for WT and APP/PS1 mice at 6, 9, and 12 months of age (Cochran-Armitage test,

2012; Nilssen et al., 2019; Rowland et al., 2018; Yao et al., 2021)—was significantly reduced in APP/PS1 compared with WT brains (Fig. 2E; Table S6). *Gfap*$^+$ neurons, on the other hand, exhibited an increase in mitochondria-dependent superoxide generation in APP/PS1 mice compared with WT mice (Fig. 2F; Table S6). Additionally, *Gfap*$^+$ neurons showed a significant reduction in synaptic functions (Fig. 2F; Table S6). These results suggest that both EC-stellate and *Gfap*$^+$ neurons influence AD pathology by jointly modulating mitochondrial function and superoxide production.

By analyzing the distribution of EC-stellate and *Gfap*$^+$ neurons in APP/PS1 and WT mice across various ages, we observed that the percentage of EC-stellate cells decreased continuously from 6M to 9M and 12M in APP/PS1 mice (Fig. 2G). Previous studies have similarly shown a reduction in the number of neurons expressing *Reln*, a marker of EC-stellate cells, in the brain of AD patients (Chin et al., 2007; Herring et al., 2012; Kobro-Flatmoen et al., 2016; Mathys et al., 2024). Our pathway analysis revealed activation of pathways related to cell death, such as "programmed cell death," "neuron death," and "positive regulation of apoptotic process" (Fig. 1H), suggesting that the reduction in EC-stellate cells may be attributed to neuronal death. In contrast, the number of *Gfap*$^+$ neurons significantly increased in APP/PS1 mice from 6M to 9M and 12M, accompanied by a decrease in synaptic functions (Fig. 2F and 2G). Importantly, we did not detect any changes in *Gfap*$^+$ neuronal numbers in WT mice with age (Fig. 2G).

To further analyze the distribution of *Gfap*$^+$ neurons in APP/PS1 and WT mice across various ages, we performed co-immunostaining of GFAP and NeuN to visualize *Gfap*$^+$ neurons. Consistent with our sequencing data, we identified *Gfap*$^+$ neurons in APP/PS1 brains (Fig. 2H). Immunofluorescence analysis also revealed that *Gfap*$^+$ neurons were significantly increased in both CA1 and CA3 regions of APP/PS1 mice from 6M to 9M and 12M, whereas only a marginal increase was observed in the hippocampus of WT mice at 12M, suggesting that *Gfap*$^+$ neurons increase with disease progression (Fig. 2H). By conducting co-immunostaining of lymphoid enhancer-binding factor 1 (LEF1), a marker of EC-stellate neurons, and NeuN, we observed a significant reduction in the percentage of EC-stellate cells in APP/PS1 mice compared with WT mice at all age stages (Fig. 2I). Moreover, EC-stellate cells showed a continuous decrease from 6M to 9M and 12M in APP/PS1 mice (Fig. 2I). Notably, we did not detect any changes in EC-stellate cell numbers in WT mice with age (Fig. 2I). These findings support the notion that AD pathology spreads from CA3 to other brain regions.

Aberrant expression of Meg3 contributes to abnormal energy metabolism of EC-HPC neurons and the death of EC-stellate cells

As demonstrated in Fig. 2E, mitochondrial respiratory function in EC-stellate neurons, which are crucial for spatial memory and have high energy demands (Crotty et al., 2012; Nilssen et al., 2019; Rowland et al., 2018; Yao et al., 2021), was significantly reduced in APP/PS1 brains compared with WT brains (Fig. 2E; Table S6). Given that genes with similar expression patterns often perform related functions, we conducted weighted gene co-expression network analysis (WGCNA) to group genes with similar expression patterns into modules and assess the correlation of these modules with cellular characteristics. Our analysis revealed that the expression of genes in the greenyellow WGCNA module was associated with the pathological progression of AD (Fig. S1C; Table S7). Genes within the greenyellow module exhibited an age-related reversal in expression patterns: their expression increased in APP/PS1 brains compared with WT brains at 6M of age, but this difference diminished by 9M of age. At 12M of age, the expression of genes in the greenyellow module became decreased in APP/PS1 brains relative to WT brains (Fig. 3A).

Notably, genes in the greenyellow module within EC-stellate cells displayed the most pronounced changes in APP/PS1 brains versus WT brains (Fig. 3A), highlighting the significant role of EC-stellate cells in AD pathology. In our co-expression network analysis of genes in this module, *maternally expressed gene* 3 (*Meg3*) emerged not only as the most significant gene correlated with AD progression but also as a major hub gene within the network (Fig. 3B and 3C). *Meg3* is a non-coding RNA produced from the *Dlk1-Gtl2* imprinted locus and is known to inhibit mitochondrial metabolism (Qian et al., 2016). We analyzed *Meg3* expression across different brain regions and ages in both APP/PS1 and WT mice and found that *Meg3* expression was significantly higher in the brains of APP/PS1 mice compared with WT mice at 6M of age (Figs. 3D and S2A). This differences in *Meg3* expression between APP/PS1 and WT mice at 6M diminished by 9M, and surprisingly, *Meg3* expression was significantly lower in the CA3 region of APP/PS1 mice compared with WT mice at 12M of age (Figs. 3D and S2A). We then examined *Meg3* expression in the identified nine neuronal clusters and found that *Meg3* expression was significantly higher in EC-stellate cells compared with other clustered neurons (Figs. 3D and S2B). Additionally, *Meg3* expression was notably higher in EC-stellate cells of APP/PS1 mice than in those of WT mice (Figs. 3D and S2B). We further validated the changes in *Meg3* expression by conducting

*$P < 0.05$; **$P < 0.01$; ***$P < 0.001$). (H) Representative immunostaining images of GFAP (green), NeuN (red), and DAPI (blue) in APP/PS1 and WT hippocampus at 6, 9, and 12 months of age. Scale bar: 100 μm. (I) Representative immunostaining images of LEF1 (red), NeuN (green), and DAPI (blue) in APP/PS1 and WT mice at the indicated ages. Scale bar: 100 μm.

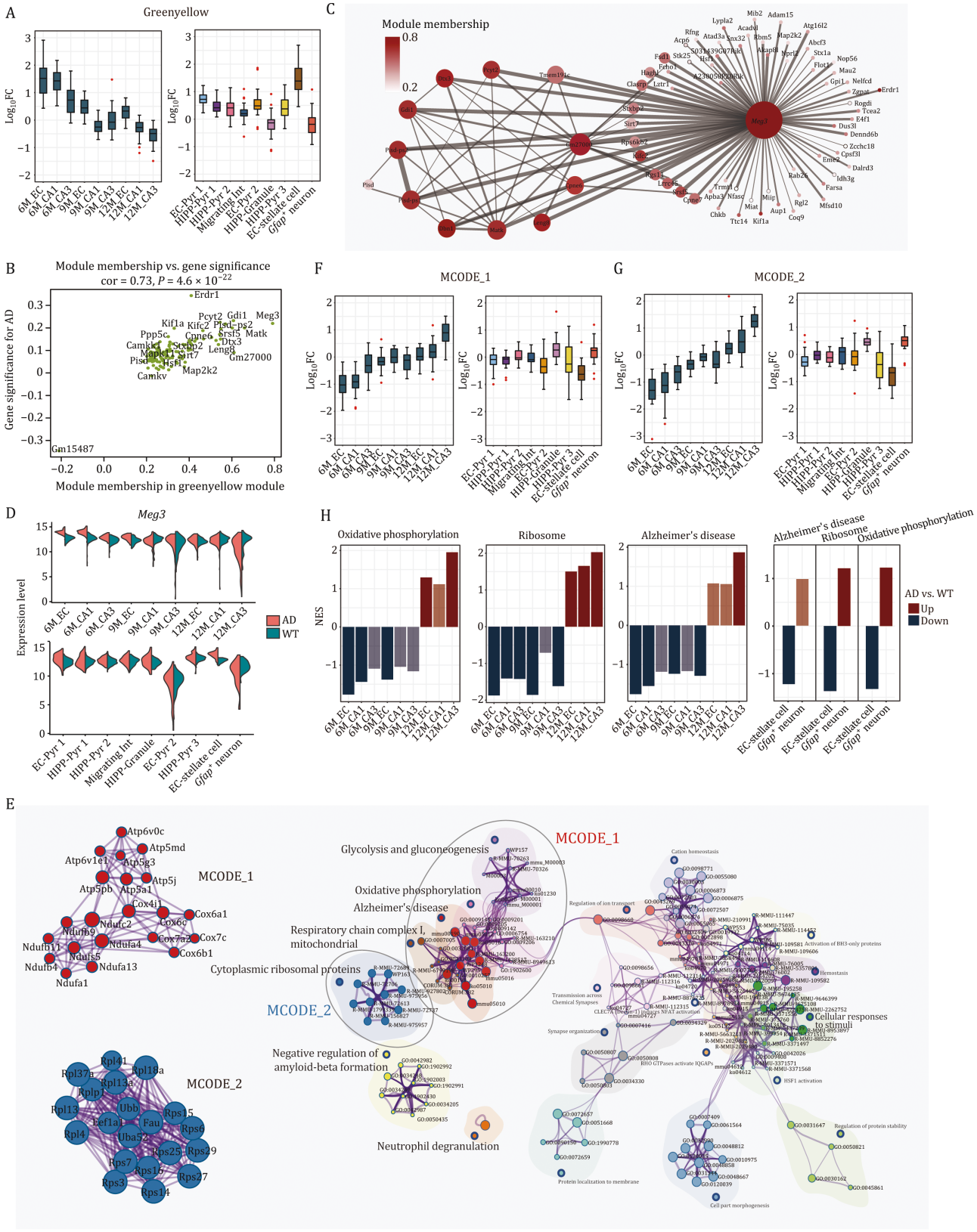

Figure 3. *Meg3* regulates energy metabolism in the EC-HPC neural circuit. (A) Expression profiles of genes in the greenyellow module altered by AD pathology, shown as $\log_{10}$ fold changes ($\log_{10}$FC) in APP/PS1 versus WT mice across the indicated ages and brain regions (left) or indicated neuronal clusters (right). (B) Correlation of greenyellow module genes with AD pathology (correlation = 0.73, $P = 4.6 \times 10^{-22}$). Genes with higher gene significance and module membership are considered key contributors. (C) Weighted gene co-expression network analysis (WGCNA) for the greenyellow module genes. The grey line indicates the presence of co-expression between genes within the module. Thickness reflects strength. Node represents module gene, and its color and size represent module membership and connectivity, respectively. (D) *Meg3* expression in the indicated brain regions and ages (upper), or neuronal

qPCR analysis and found that *Meg3* levels were significantly increased in APP/PS1 mice compared with control WT mice at 6M (Fig. S1E). These findings suggest that aberrant expression of *Meg3*, particularly in EC-stellate cells, is closely associated with the progression of AD.

We next investigated genes that are negatively correlated with *Meg3* expression. We selected the top 200 genes with the strongest negative correlations for pathway analysis. This analysis revealed that these genes were functionally associated with mitochondria and ribosomes, whose dysfunction is known to contribute to the pathological features of AD (Fig. S1F). MCODE analysis identified two major complexes: the mitochondrial oxidative phosphorylation-related gene set (MCODE 1) and the ribosome-related gene set (MCODE 2) (Fig. 3E). Notably, the expression of genes in both MCODE 1 and MCODE 2 decreased in APP/PS1 brains compared with WT brains at 6M of age, remained largely unchanged at 9M of age, and increased at 12M of age in APP/PS1 brains relative to WT brains (Fig. 3F and 3G). Consistent with these findings, pathways related to oxidative phosphorylation, ribosomes, and Alzheimer's disease transitioned from repression to activation from 6M and 9M to 12M in APP/PS1 mice compared with WT mice (Fig. 3H). Specifically, these pathways were repressed in EC-stellate cells and activated in *Gfap*$^+$ neurons at 12M of age (Fig. 3H). Collectively, these results suggest that *Meg3* regulates mitochondrial respiratory and ribosomal functions by altering the expression of these genes. Thus, the reduction of EC-stellate cells in APP/PS1 mice likely contributes to AD pathology through *Meg3*-mediated dysfunction in the mitochondrial respiratory and ribosomes.

Glia- and stem cell-like features in disease-associated *Gfap* neurons contribute to AD progression

Glial fibrillary acidic protein (GFAP) is a well-established marker for glial cells. Previous studies have linked GFAP expression to AD pathology, suggesting astrocyte activation in AD (Benedet et al., 2021; Johansson et al., 2023; O'Connor et al., 2023; Pereira et al., 2021). In this study, we identified a subpopulation of neurons expressing *GFAP* in APP/PS1 mice (Fig. 4A). We observed a significant increase in both the number of neurons expressing *GFAP* and the neuronal expression levels of *GFAP* in APP/PS1 mice compared with WT mice (Figs. 4A, 4B, and S2G). Immunostaining with anti-Map2 and anti-GFAP antibodies not only confirmed the presence of GFAP$^+$ neurons in the brains of APP/PS1 mice but also demonstrated an increase in both the GFAP$^+$ neurons and the GFAP signal per neuron in the CA3, CA1, and EC regions of APP/PS1 mice compared with age-matched WT brains (Fig. 4C). This suggests that a subset of neurons expresses GFAP under AD pathological conditions, contributing to AD pathology.

In addition to *Gfap*, these neurons also express other typical glial markers, such as *Aqp4* and *Mbp*, as well as stem cell markers such as *Hopx*, *Vim*, and *Sox9* (Fig. 4B). Interestingly, these neurons showed reduced expression of neuronal markers, including *Gad1*, *Syt1*, and *Grin2b* (Fig. 4B). GO analysis revealed that these neurons are functionally related to gliogenesis and glial differentiation (Fig. 4D). Therefore, we have renamed this subset of neurons as disease-associated *Gfap*$^+$ neurons. Through WGCNA, we identified a co-expression module gene set, termed "yellow," which mirrors the molecular characteristics of *Gfap*$^+$ neurons (Fig. S1G; Table S7).

We next simulated the cellular states of *Gfap*$^+$ neurons and investigated their transition during AD progression. Trajectory analysis divided *Gfap*$^+$ neurons into three distinct states: state 1, state 2, and state 3 (Fig. 4E). In the context of AD pathology, state 1 predominantly represented WT conditions (AD/WT: 1/12), state 2 represented both AD and WT conditions (AD/WT: 7/8), and state 3 primarily represented AD conditions (AD/WT: 19/3) (Fig. 4E). In terms of age, state 1 was most characteristic of 6M, state 2 of 9M, and state 3 of 12M (Fig. 4E). Thus, the trajectory features of cell state transitions effectively reflect the pathological progression in APP/PS1 mice. GSEA revealed that state 3 neurons exhibited upregulated pathways related to mitochondrial oxidative phosphorylation, reactive oxygen species (ROS), and glial cell differentiation, whereas state 1 neurons were associated with pathways such as dendritic spine morphology and glutamate receptor signaling (Fig. 4F and 4G). These findings indicate that *Gfap*$^+$ neurons are closely linked to AD pathology, with the state 3 subtype of *Gfap*$^+$ neurons representing the advanced stage of AD progression.

We further observed that the *Gfap* expression was associated with the state of *Gfap*$^+$ neurons. Specifically, *Gfap* expression exhibited a minor increase during the transition from state 1 to state 2 and a sharp increase during the transition from state 2 to state 3 (Fig. 4F). In addition, the state of *Gfap*$^+$ neurons was influenced by the expression of specific genes. We found that ApoE expression demonstrated a linear correlation with state transitions (Figs. 4F and S1H). Moreover, neuronal markers such as *Syt1* and *Snap25* consistently showed a negative

clusters (lower) between APP/PS1 and WT mice. (E) Pathway network analysis for the top 200 genes negatively correlated with *Meg3* expression. Distinct pathways are color-coded (e.g., MCODE1: mitochondrial, red; MCODE2: ribosomal, blue), with nodes representing subpathways. (F and G) $Log_{10}FC$ of genes enriched in MCODE1 (F) and MCODE2 (G) networks in the indicated brain regions and ages, or neuronal clusters. (H) Normalized Enrichment Score (NES) for oxidative phosphorylation, ribosome, and AD pathways in APP/PS1 versus WT mice at the indicated ages and brain regions, within EC-stellate or *Gfap*$^+$ neurons.

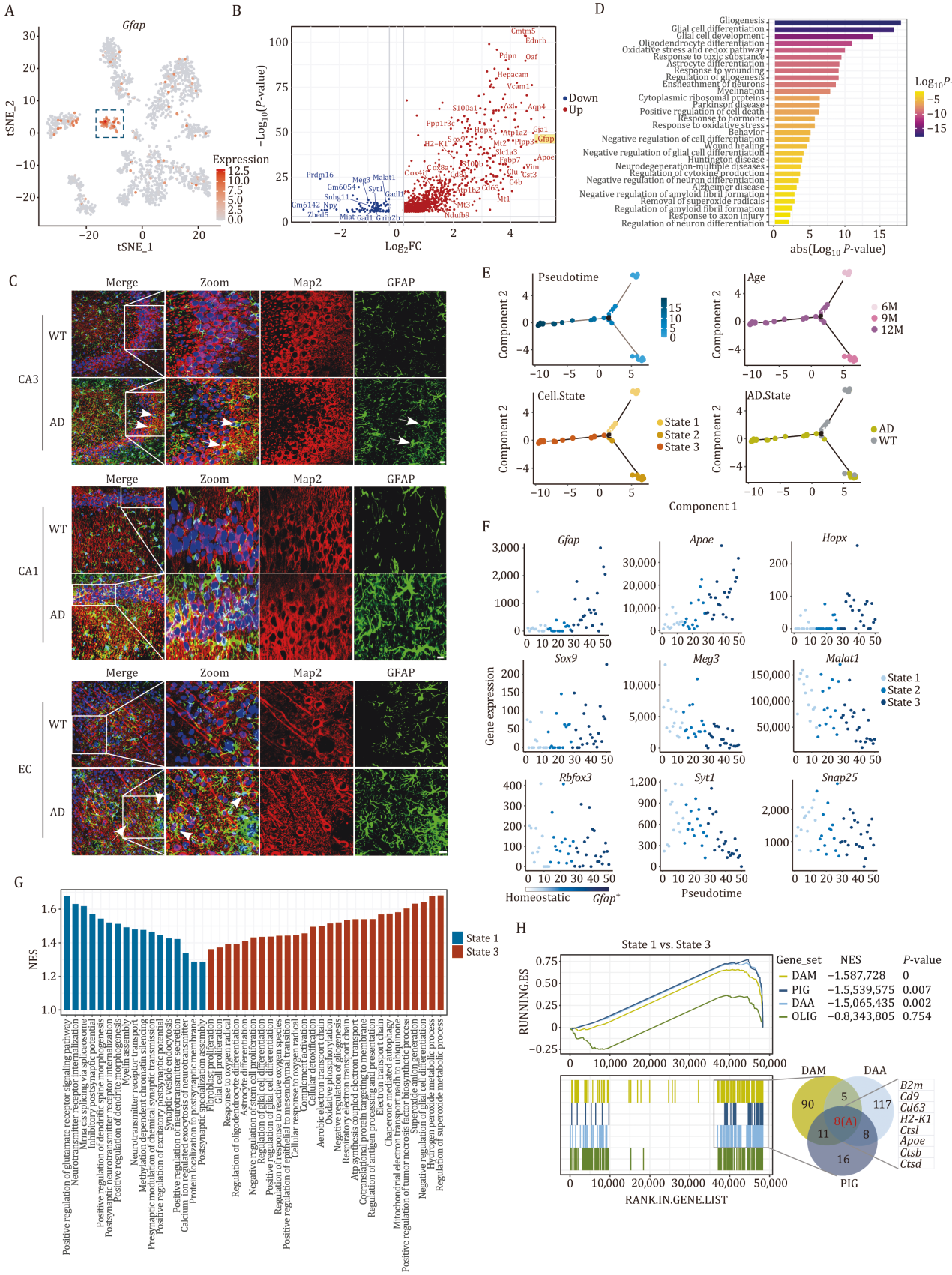

Figure 4. Characterization of *Gfap*⁺ neurons in AD pathology. (A) t-SNE visualization of *Gfap* expression in neuronal clusters (from Fig. 1C). Square denotes *Gfap*⁺ neurons. (B) Volcano plot to visualize DEGs in *Gfap*⁺ neurons versus all other neuronal types. (C) Representative immunofluorescence images of GFAP (green), Map2 (red), and DAPI (blue) in the CA3, CA1, and EC of 12-month-old WT and APP/PS1 mice. Scale bars, 20 μm. (D) Functional enrichment of signature genes in *Gfap*⁺ neurons. (E) Pseudotime trajectory of *Gfap*⁺ neurons across pathological progression. (F) Expression dynamics of representative genes in GFAP⁺ neurons over pseudotime,

correlation with the transitions from state 1 to both state 2 and state 3 (Fig. 4F). This observation aligns with the higher neuronal functionality in state 1 compared with the other states (Fig. 4G). Furthermore, the stem cell markers displayed expression patterns similar to *Gfap*: a minor increase during the transition from state 1 to state 2 and a pronounced increase during the transition from state 2 to state 3 (Fig. 4F). These findings suggest that the reprogramming of cell states from neuron-like to glia-like and stem-like is closely associated with AD progression. Moreover, both lncRNA *Malat1* and *Meg3* exhibited negative correlation with transitions from state 1 to state 2 and state 3 (Figs. 4F and S1H), reflecting changes in mitochondrial and ribosomal functions during AD progression (Fig. 4G).

We further analyzed state 1 and state 3 neurons along the trajectory to identify the enrichment of marker genes associated with disease-associated microglia (DAM; Keren-Shaul et al., 2017), with disease-associated astrocytes (DAA; Habib et al., 2020), with plaque-induced genes (PIG; Chen et al., 2020), and with oligodendrocyte genes (OLIG; Kenigsbuch et al., 2022). Our analysis revealed that state 3 neurons showed higher expression of marker genes for DAM, DAA, and PIG, but not for OLIG, compared with state 1 neurons (Fig. 4H). We identified eight overlap genes that were abundantly expressed in state 3 neurons but not in state 1 neurons, including *B2m*, *Cd9*, *Cd63*, *H2-K1*, *Ctsl*, *Apoe*, *Ctsb*, and *Ctsd* (Fig. 4H). These findings suggest that state 3 neurons exhibit disease-associated characteristics, contributing to AD progression.

Increase in neuronal GFAP expression is a shared pathological feature among AD model mice and AD patients

APP23 transgenic mice express the 751 isoform of human APP harboring the double Swedish mutation, driven by the Thy-1.2 promoter (Sturchler-Pierrat et al., 1997). Compared with the dual-transgenic APP/PS1 model, APP23 transgenic mice exhibit a delayed onset of pathological phenotypes (Pádua et al., 2024). By employing APP23 transgenic mice, we also identified the presence of *Gfap*$^+$ neurons and observed an increase in their numbers in the hippocampal CA1 and CA3 regions of APP23 transgenic mice, compared with control WT mice (Fig. 5A and 5B). This finding was confirmed through the analysis of previously published single-cell transcriptome sequencing data (Zhong et al., 2020). To ensure a consistent sampling across different brain regions, we excluded neurons derived from the hippocampal dentate gyrus by removing those neurons with prox1 expression (prox1 > 0), as prox1 is a marker gene for dentate gyrus neurons. Our analysis revealed that *Gfap*$^+$ neurons in the CA1 and CA3 regions accounted for 1.8% of the total neurons isolated from APP23 transgenic mice at 6M of age and 9.6% at 24M of age. In contrast, these neurons represented 0.8% of total neurons in WT mice at 6M of age and 3.4% at 24M (Fig. 5B). These results further confirm that *Gfap*$^+$ neuron number significantly increases as AD progresses.

By analyzing the single-cell datasets from the EC region of AD patients (Grubman et al., 2019), we confirmed the presence of *GFAP*$^+$ neurons in human AD cases (Fig. 5C and 5D). We extracted neuronal data from the human dataset and identified a neuronal subpopulation, n1, which exhibited specific and higher expression of *GFAP* (Fig. 5C and 5D). Further analysis showed that the n1 subpopulation neurons had a higher gene set enrichment score (AUC score) for genes in the yellow module compared with other subpopulations, indicating that these genes are preferentially enriched at the top ranking for n1 neurons (Fig. 5E). Additionally, we found that 95% of n1 neurons were derived from AD patients, while only 5% of n1 neurons came from control patients (Fig. 5F). This suggests that n1 neurons are associated with pathological progression. Thus, the presence of *GFAP*$^+$ neurons is a common pathological feature in both AD mice and human patients.

In addition to elevated *GFAP* expression, *GFAP*$^+$ neurons derived from human datasets (n1) also showed reduced levels of neuronal signature genes, including *RBFOX1*, *RBFOX3*, *SYT1*, and *SNAP25*, as well as decreased expression of lncRNAs such as *MALAT1* and *Meg3* (Fig. 5G and 5H). Pathway analysis revealed significant enrichment in processes related to gliogenesis and glial cell differentiation in *GFAP*$^+$ neurons (Fig. 5I). These findings are consistent with the characteristics of *GFAP*$^+$ neurons observed in APP/PS1 mice (Fig. 4B and 4G). We further examined human brain samples and identified a similar subpopulation of neurons (n1) with elevated *GFAP* expression compared with other neuronal subpopulations (n2–n6) (Fig. 5J). We quantified the proportion of *GFAP*$^+$ neurons in AD patients versus controls and found that, in the AD patient group, *GFAP*$^+$ neurons comprised 38% of the total neurons. In contrast, the control group had only 2% *GFAP*$^+$ neurons, with the highest proportion observed in C1, which was the only sample with occasional diffuse plaques in the cortex (Table S8, Ct1_Ct2 donor 1) (Fig. 5K). These results indicate a specific increase in *GFAP*$^+$ neurons in AD patients.

In summary, we have demonstrated that the number of EC-stellate neurons in the EC-HPC circuit reduces

including astrocytic genes (*Gfap*, *Apoe*), stem genes (*Hopx*, *Sox9*, *Notch2*, *Vim*), neuronal genes (*Rbfox3*, *Syt1*, *Snap25*), and lncRNAs (*Malat1*, *Meg3*). (G) GSEA comparing state1 and state3 *GFAP*$^+$ neurons. (H) GSEA of DAM, DAA, PIG, and OLIG gene sets in state 1 versus state 3 *Gfap*$^+$ neurons. State 3 neurons showed significant enrichment in DAM, DAA, and PIG gene sets (NES > 1, $P < 0.05$), but not OLIG (NES < 1, $P > 0.05$), compared with state 1 neurons.

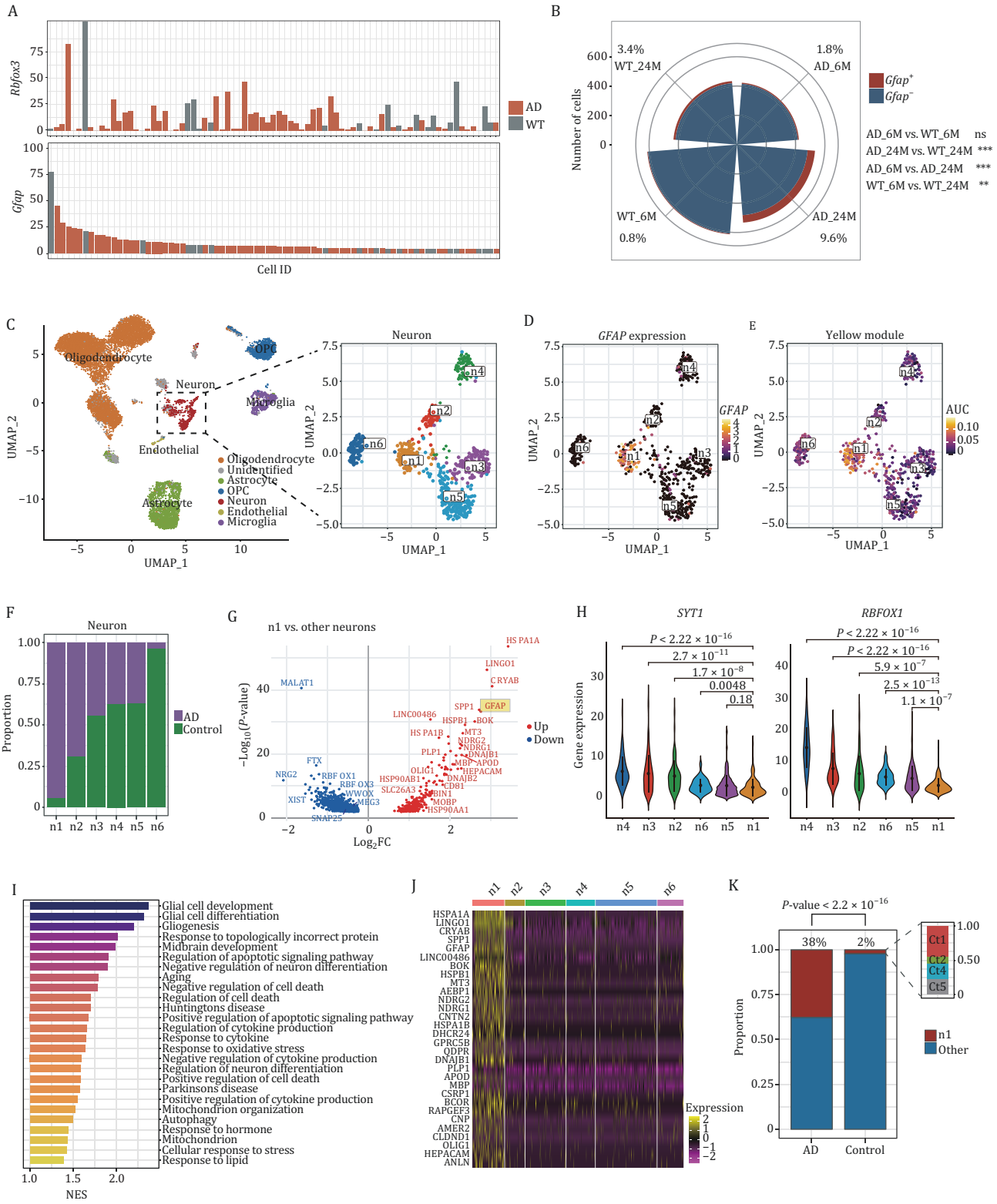

Figure 5. Identification and characterization of *GFAP*⁺ neurons in human dataset. (A) Expression levels of *Rbfox3* and *Gfap* in neurons from APP23 and WT mice (Zhong et al., 2020), with *Gfap* expression count > 3. The *x*-axis represents cell IDs sorted in descending order of *Gfap* expression. (B) Proportion of *Gfap*⁺ neurons in the hippocampus of APP23 and WT mice (Zhong et al., 2020). Chi-square test: ns, not significant; $^{**}P < 0.01$; $^{***}P < 0.001$. (C) Clustering analysis of neurons from human dataset (Grubman et al., 2019). (D) *GFAP* expression levels across neuronal clusters in the human dataset (Grubman et al., 2019). (E) Uniform manifold approximation and projection of neurons in human dataset, based on AUC scores derived from the yellow module of our APP/PS1 dataset. (F) Proportion of control and AD patients in each cluster identified in (E). (G) Volcano plot showing DEGs in n1 cluster neurons versus all other clusters. (H) Expression of *SYT1* and *RBFOX1* (neuronal markers) across identified clusters in human neurons. (I) Functional enrichment of n1 cluster signature genes. (J) Heatmap showing the expression of signature genes across n1–n6 neuron clusters. (K) Distribution of n1 and other cluster neurons in control versus AD patients (Chi-square test).

during AD progression, leading to dysfunction in energy metabolism. We have further identified a subpopulation of disease-associated neurons that exhibit a loss of neuron-like features and an emergence of both glial and stem-like characteristics. The increase in this disease-associated neuronal population may be a key factor or specific cellular manifestation of the neurodegenerative changes observed in AD pathology.

Discussion

AD is a progressive neurodegenerative disorder. Notably, neurons exhibit selective vulnerability to AD pathology, which is dependent not only on the disease stage but also on neuronal subtypes and distributions (Braak and Braak, 1990; Grøntvedt et al., 2018; Igarashi, 2023; Jun et al., 2020; Kunz et al., 2015; Moser et al., 2015; Yao et al., 2021; Ying et al., 2022). Previous research has mostly focused on comparing diseased and healthy brains at endpoint stage. Our study took a more comprehensive approach and created extensive molecular profiles. By conducting Smart-seq2 single-cell technology, we investigated differential gene expression across various disease stages within the EC-HPC neuronal circuit, a region highly sensitive to the AD pathology. Our dataset consists of 1,663 single-cell transcriptomes, spanning three stages (early, middle, and late), and three regions within the EC-HPC circuit (EC, hippocampal CA1, and CA3).

Compared with the more commonly used droplet-based 10x technique, Smart-seq2 offers greater sensitivity for single-nucleus-based RNA-seq analysis (Mereu et al., 2020; Ziegenhain et al., 2017). This technique captures a substantially higher number of genes per cell, including low-abundance and alternatively spliced transcripts (Ziegenhain et al., 2017). The optimal balance between the number of cells and their sequencing depth depends on the scientific questions addressed. When accurate single-cell transcriptome annotation was a primary goal, Smart-seq2 was the most suitable approach. The sequencing depth per nucleus in this study was comparable to the average reads per sample for bulk RNA-seq, making it well-suited for detailed transcriptome annotation. Regarding cell numbers, simulations have shown that Smart-seq2 requires ~100 cells at one million reads to achieve 80% power for detecting differentially expressed genes (Ziegenhain et al., 2017). In neuroscience research, Smart-seq2-based studies typically include a few hundred cells (Kalamakis et al., 2019; Li et al., 2022). Therefore, the nucleus count in this study is sufficient to effectively survey cell-type diversity during AD progression.

Brain is a highly energy-demanding organ and is particularly sensitive to disturbances in energy metabolism (Bélanger et al., 2011). As the primary site of energy production, the mitochondria play a critical role in sustaining neuronal function. Aberrant energy metabolism and mitochondrial dysfunction are recognized hallmarks of aging brains and are further exacerbated in AD brains (He et al., 2024; Jin et al., 2024; Kerr et al., 2017; Venkataraman et al., 2022; Yin et al., 2016; Zhang et al., 2024). However, the underlying cellular and molecular mechanisms remain largely elusive. By analyzing AD and WT mice at of 6, 9, and 12 months of age, we demonstrate that mitochondrial function is suppressed during the early stages of AD pathology, even before the appearance of amyloid deposition, particularly in the EC. This early mitochondrial dysfunction may contribute to neuronal loss in the EC, consistent with the region's heightened vulnerability to AD pathology. As the disease progresses, we observed a subsequent activation of mitochondrial function. This late-stage activation may represent a compensatory response to escalating damage, including Aβ plaque deposition and neuroinflammation. In summary, our study delineates the dynamic changes in energy metabolism throughout AD progression, offering valuable insights into the potential use of energy metabolism as a diagnostic and prognosis biomarker for AD pathology.

Meg3 is known to regulate mitochondrial function by interacting with pathways involved in mitochondrial biogenesis, dynamic, and metabolism. Dysregulation in Meg3 expression can lead to mitochondrial dysfunction, resulting in reduced ATP production and increased ROS levels, thereby exacerbating oxidative stress and contributing to neuronal damage in AD pathology (Qian et al., 2016). Aberrant Meg3 expression has been extensively reported in AD pathology (Baazaoui et al., 2025; Balusu et al., 2023; Yi et al., 2019; Zhang et al., 2021), often accompanied by mitochondrial dysfunction and disrupted energy metabolism. These findings are consistent with our observations in this study, where we identified a co-occurrence of aberrant Meg3 expression and impaired energy metabolism during AD progression. We further demonstrate that Meg3 expression undergoes dynamic changes with AD progression, which are associated with distinct patterns of metabolic disturbances. Our study suggests that Meg3 may act as a critical regulatory switch in controlling neuronal energy metabolism during AD pathology.

Of note, the expression pattern of Meg3 in AD pathology appear to be controversial and inconsistent across published studies (Baazaoui et al., 2025). This variability may be due to differences in the specific brain regions and disease stages analyzed. By conducting temporal spatial single-cell transcriptome analysis, we demonstrate that Meg3 is specifically expressed in EC-stellate neurons, with a substantial increase in these neurons, particularly in the early stage of AD. This increase is considered detrimental to EC-stellate neurons, as previous studies have shown that Meg3 expression can induce

necroptotic apoptosis in cultured neurons, while reduction in Meg3 expression rescues neuronal loss in xenografted human neurons (Balusu et al., 2023). Notably, the upregulation of Meg3 expression was most pronounced in the EC and CA1 regions during the early stage of AD, which may explain their heightened vulnerability to AD pathology. As the disease progresses, the upregulation of Meg3 becomes less significant, likely due to neuronal loss. Thus, we demonstrate that Meg3 expression is both brain region- and disease stage-dependent, suggesting that it could serve as a prognosis marker for AD pathology. Targeting Meg3 expression at specific pathological stages could provide a promising therapeutic strategy to prevent early neuronal death in AD.

GFAP is an intermediate filament protein predominantly found in astrocytes and is commonly used as a marker of reactive astrocytes (Benedet et al., 2021; Johansson et al., 2023; O'Connor et al., 2023; Pereira et al., 2021). The expression of *GFAP* is consistently elevated in the brains of AD patients, with levels correlating closely with AD-related pathology and disease progression. Recently, the National Institute on Aging and the Alzheimer's Association included GFAP as a recommended biomarker in the latest revised clinical criteria for Alzheimer's disease (Jack Jr et al., 2024). It is widely recognized that astrocytic activation is associated with the progression of AD pathology.

Astrocytes become activated and reactive during AD progression, a process known as astrogliosis. Astrogliosis is characterized by increased astrocyte size, proliferation, and increased expression of the astrocyte marker protein GFAP. Reactive astrocytes have both beneficial (neuroprotective) and detrimental (neurotoxic) effects depending on their reactivity profile. The neurotoxic form of astrocytes is induced by cytokines such as complement factors (C1q), TNF-α, and IL-1α, and is abundantly present in various neurodegenerative diseases (Liddelow et al., 2017), and 30%–60% of astrocytes in degenerative brains exhibit a neurotoxic phenotype, which is hypothesized to play a critical role in disease initiation and progression (Liddelow et al., 2017). In contrast, neuroprotective form of astrocytes is associated with increased expression of several neuroprotective factors, including prokineticin-2 (PK2), chitin-like 3, frizzled class receptor 1, Nrf2, pentraxin 3 (PTX3), sphingosine kinase 1, and transmembrane 4 L6 family member 1, promoting synaptic repair and neuronal survival (Liddelow et al., 2017). Reactive astrocytes play dual roles in AD pathology, where they may initially be involved in active clearance of Aβ plaque. However, as Aβ deposition accumulates with AD progression, their protective functions may diminish, leading to a loss of homeostasis and the spreading of Aβ pathology (Edison, 2024). Beyond the traditional view of reactive astrocytes existing a simple binary state, recent single-nucleus transcriptome analyses have identified transcriptionally diverse astroglial subpopulations exhibiting disease-specific changes (Habib et al., 2020; Lau et al., 2020). While *GFAP* expression remains a hallmark of reactive astrocytes, a more comprehensive analysis of other gene expression changes is essential to accurately define their states.

In this study, we identified a novel subtype of neurons that unexpectedly express *GFAP*. This aberrant *GFAP* expression appear to be a shared pathological feature in both astrocytes and neurons during AD progression. In addition to *GFAP*, these neurons exhibit a similar gene expression profile to disease-associated astrocytes, suggesting a conversion of neuronal cell states in response to pathological damage. Unlike reactive astrocytes, we propose that this state conversion in neurons is primarily detrimental to their function, contributing to neurodegeneration.

In addition to *GFAP* expression, other astrocytic genes, such as ApoE, were found to be abundantly expressed in the novel subtype of neurons identified in this study. This suggests that neuronal ApoE expression is closely associated with AD pathology. Previous studies have supported this by demonstrating that neuronal ApoE expression serves as a robust genetic link to AD pathology (Zalocusky et al., 2021). By establishing connections between neuronal ApoE expression and immune-response pathways, this study suggests that neuronal ApoE may play a causal role in neurodegenerative diseases and could potentially serve as a marker to track disease progression (Zalocusky et al., 2021).

In addition to expressing astrocytic marker genes, GFAP$^+$ neurons also express stem-like genes while losing the expression of neuronal marker genes, such as NeuN and *Snap25*. These findings indicate that this *Gfap*-expressing neurons surrender their neuronal identity and function. Neurons that lose their identity may adopt a more primitive or dysfunctional state, making them more susceptible to neurodegeneration. When neurons loss their neuronal markers, they may struggle to form new synaptic connections, leading to impaired synapse plasticity, defective synaptic function, and disrupted memory formation. The acquisition of non-neuronal markers in neurons may indicate a form of neuronal conversion or a reactive response to injury. This loss of neuronal is often first observed in vulnerable regions, such as the hippocampus and cortex, as demonstrated in this study, leading to a manifestation of neurodegeneration and synapse loss during the pathological process. Moreover, a significant activation of PIG genes in *Gfap*$^+$ neurons, along with the detection of *GFAP*$^+$ neurons in human brain samples with occasional diffuse plaques, support a strong association between *GFAP*$^+$ neurons and AD pathology.

Overall, our study demonstrates that up to 38% of neurons undergo a transformation into *GFAP*-expressing

neurons in the EC region of postmortem AD patients. This pathological shift, which extensively affects neurons across the EC-HPC circuit, likely plays a critical role in the late-stage progression of AD, contributing to neurofunctional decline and cognitive impairment. Targeting the restoration of neuronal characteristics and functions in *GFAP*-expressing neurons may present a potential therapeutic approach to reverse the neurodegenerative phenotype of AD and improve cognitive function.

Supplementary data

Supplementary data is available at *Protein & Cell* online https://doi.org/10.1093/procel/pwaf042.

Acknowledgements

We thank Professors Zhengang Yang and Zhiqiang Dong for their guidance on this study. We thank China National GeneBank for providing sequencing services for this project.

Conflict of interest

The authors declare no competing interests.

Funding

This research was supported by the National Natural Science Foundation of China (Grant Nos. 82125009, 82330045, 32121002, 82071185, 82172061, and 92149303), the National Key R&D Program of China (Grant Nos. 2020YFA0509300, 2021YFA0804900, and 2022YFC2703102), the Strategic Priority Research Program of the Chinese Academy of Sciences (XDB39000000), CAS Project for Young Scientists in Basic Research (YSBR-013), Plans for Major Provincial Science & Technology Projects (202303a07020004), Hefei Comprehensive National Science Center Hefei Brain Project, Research Funds of Center for Advanced Interdisciplinary Science and Biomedicine of IHM (QYZD20220003), the Major Frontier Research Project of the University of Science and Technology of China (LS9100000002), and S&T Program of Shijiazhuang (235790429H).

Code availability statement

All the custom code is available from the corresponding authors upon reasonable request.

Author contributions

Q.L., J.Z., and JG.Z. conceived the project and designed the study. Y.M., S.G., and H.L. designed and performed bioinformatic analysis. D.L., and L.W performed experiments. Q.L., J.Z., Y.M., and JG.Z. interpreted results. Y.M., J.Z., and Q.L. wrote the manuscript. Y.M., S.G., and S.Y. contributed to the data visualization. J.H. prepared the graphic abstract. Q.L., J.Z., X.S., X.L., AS., Y.G., N.Z., and Y.P. revised the manuscript. L.Z., G.L., W.W., S.Z., H.Y., and J.W. contributed to project design. All authors have read and approved the final manuscript.

Ethics approval

All animal procedures were approved by and performed in accordance with the guidelines of the Institutional Animal Care and Use Committee of University of Science and Technology of China.

Consent to participate

All authors give their consent to participate.

Consent for publication

All authors give their consent to publication.

Artificial intelligence

Not applicable.

Data availability

The data that support the findings of this study have been deposited in the CNSA of China National GeneBank DataBase (CNGBdb) with accession code CNP CNP0003770.

References

Arendash GW, King DL, Gordon MN *et al*. Progressive, age-related behavioral impairments in transgenic mice carrying both mutant amyloid precursor protein and presenilin-1 transgenes. *Brain Res* 2001;**891**:42–53.

Baazaoui N, Y Alfaifi M, Ben Saad R *et al*. Potential role of long noncoding RNA maternally expressed gene 3 (MEG3) in the process of neurodegeneration. *Neuroscience* 2025;**565**:487–498.

Balusu S, Horré K, Thrupp N *et al*. MEG3 activates necroptosis in human neuron xenografts modeling Alzheimer's disease. *Science (New York, N.Y.)* 2023;**381**:1176–1182.

Bélanger M, Allaman I, Magistretti PJ. Brain energy metabolism: focus on astrocyte-neuron metabolic cooperation. *Cell Metab* 2011;**14**:724–738.

Benedet AL, Milà-Alomà M, Vrillon A *et al*; Translational Biomarkers in Aging and Dementia (TRIAD) study, Alzheimer's and Families (ALFA) study, and BioCogBank Paris Lariboisière cohort. Differences between plasma and cerebrospinal fluid glial fibrillary acidic protein levels across the Alzheimer disease continuum. *JAMA Neurol* 2021;**78**:1471–1483.

Bergmann T, Liu Y, Skov J *et al*. Production of human entorhinal stellate cell-like cells by forward programming shows an important role of Foxp1 in reprogramming. *Front Cell Dev Biol* 2022;**10**:976549.

Braak H, Braak E. Neurofibrillary changes confined to the entorhinal region and an abundance of cortical amyloid in cases of presenile and senile dementia. *Acta Neuropathol* 1990;**80**:479–486.

Chen W-T, Lu A, Craessaerts K *et al*. Spatial transcriptomics and in situ sequencing to study Alzheimer's disease. *Cell* 2020;**182**:976–991.e19.

Chin J, Massaro CM, Palop JJ *et al*. Reelin depletion in the entorhinal cortex of human amyloid precursor protein transgenic mice and humans with Alzheimer's disease. *J Neurosci* 2007;**27**:2727–2733.

Crotty P, Lasker E, Cheng S. Synchronization of entorhinal cortex stellate cells. *BMC Neurosci* 2012;**13**:1–2.

Edison P. Astroglial activation: current concepts and future directions. *Alzheimer's Dementia* 2024;**20**:3034–3053.

Grøntvedt GR, Schröder TN, Sando SB *et al*. Alzheimer's disease. *Curr Biol* 2018;**28**:R645–R649.

Grubman A, Chew G, Ouyang JF *et al*. A single-cell atlas of entorhinal cortex from individuals with Alzheimer's disease reveals cell-type-specific gene expression regulation. *Nat Neurosci* 2019;**22**:2087–2097.

Habib N, Mccabe C, Medina S *et al*. Disease-associated astrocytes in Alzheimer's disease and aging. *Nat Neurosci* 2020;**23**:701–706.

He K, Zhao Z, Zhang J *et al*. Cholesterol metabolism in neurodegenerative diseases. *Antioxidants Redox Signal* 2024;**41**:1051–1072.

Herring A, Donath A, Steiner KM *et al*. Reelin depletion is an early phenomenon of Alzheimer's pathology. *J Alzheimer's Dis* 2012;**30**:963–979.

Holtzman DM, Morris JC, Goate AM. Alzheimer's disease: the challenge of the second century. *Sci Transl Med* 2011;**3**:77sr1.

Igarashi KM. Entorhinal cortex dysfunction in Alzheimer's disease. *Trends Neurosci* 2023;**46**:124–136.

Jack Jr CR, Andrews SJ, Beach TG *et al*. Revised criteria for the diagnosis and staging of Alzheimer's disease. *Nat Med* 2024;**30**:2021–2024.

Jin S, Lu W, Zhang J *et al*. The mechanisms, hallmarks, and therapies for brain aging and age-related dementia. *Sci Bull* 2024;**69**:3756–3776.

Johansson C, Thordardottir S, Laffita-Mesa J *et al*. Plasma biomarker profiles in autosomal dominant Alzheimer's disease. *Brain* 2023;**146**:1132–1140.

Jun H, Bramian A, Soma S *et al*. Disrupted place cell remapping and impaired grid cells in a knockin model of Alzheimer's disease. *Neuron* 2020;**107**:1095–1112.e6.

Kalamakis G, Brüne D, Ravichandran S *et al*. Quiescence modulates stem cell maintenance and regenerative capacity in the aging brain. *Cell* 2019;**176**:1407–1419.e14.

Kenigsbuch M, Bost P, Halevi S *et al*. A shared disease-associated oligodendrocyte signature among multiple CNS pathologies. *Nat Neurosci* 2022;**25**:876–886.

Keren-Shaul H, Spinrad A, Weiner A *et al*. A unique microglia type associated with restricting development of Alzheimer's disease. *Cell* 2017;**169**:1276–1290.e17.

Kerr JS, Adriaanse BA, Greig NH *et al*. Mitophagy and Alzheimer's disease: cellular and molecular mechanisms. *Trends Neurosci* 2017;**40**:151–166.

Kobro-Flatmoen A, Nagelhus A, Witter MP. Reelin-immunoreactive neurons in entorhinal cortex layer II selectively express intracellular amyloid in early Alzheimer's disease. *Neurobiol Dis* 2016;**93**:172–183.

Kunz L, Schröder TN, Lee H *et al*. Reduced grid-cell–like representations in adults at genetic risk for Alzheimer's disease. *Science* 2015;**350**:430–433.

Lau S-F, Cao H, Fu AKY *et al*. Single-nucleus transcriptome analysis reveals dysregulation of angiogenic endothelial cells and neuroprotective glia in Alzheimer's disease. *Proc Natl Acad Sci USA* 2020;**117**:25800–25809.

Leng K, Li E, Eser R *et al*. Molecular characterization of selectively vulnerable neurons in Alzheimer's disease. *Nat Neurosci* 2021;**24**:276–287.

Li L, Fang F, Feng X *et al*. Single-cell transcriptome analysis of regenerating RGCs reveals potent glaucoma neural repair genes. *Neuron* 2022;**110**:2646–2663.e6.

Liddelow SA, Guttenplan KA, Clarke LE *et al*. Neurotoxic reactive astrocytes are induced by activated microglia. *Nature* 2017;**541**:481–487.

Mathys H, Davila-Velderrain J, Peng Z *et al*. Single-cell transcriptomic analysis of Alzheimer's disease. *Nature* 2019;**570**:332–337.

Mathys H, Boix CA, Akay LA *et al*. Single-cell multiregion dissection of Alzheimer's disease. *Nature* 2024;**632**:858–868.

Mereu E, Lafzi A, Moutinho C *et al*. Benchmarking single-cell RNA-sequencing protocols for cell atlas projects. *Nat Biotechnol* 2020;**38**:747–755.

Moser M-B, Rowland DC, Moser EI. Place cells, grid cells, and memory. *Cold Spring Harbor Perspect Biol* 2015;**7**:a021808.

Nilssen ES, Doan TP, Nigro MJ *et al*. Neurons and networks in the entorhinal cortex: a reappraisal of the lateral and medial entorhinal subdivisions mediating parallel cortical pathways. *Hippocampus* 2019;**29**:1238–1254.

O'connor A, Abel E, Benedet AL *et al*. Plasma GFAP in presymptomatic and symptomatic familial Alzheimer's disease: a longitudinal cohort study. *J Neurol Neurosurgery Psychiatry* 2023;**94**:90–92.

Pádua MS, Guil-Guerrero JL, Prates JA *et al*. Insights on the use of transgenic mice models in Alzheimer's disease research. *Int J Mol Sci* 2024;**25**:2805.

Pereira JB, Janelidze S, Smith R *et al*. Plasma GFAP is an early marker of amyloid-β but not tau pathology in Alzheimer's disease. *Brain* 2021;**144**:3505–3516.

Qian P, He XC, Paulson A *et al*. The Dlk1-Gtl2 locus preserves LT-HSC function by inhibiting the PI3K-mTOR pathway to restrict mitochondrial metabolism. *Cell Stem Cell* 2016;**18**:214–228.

Rosenberg AB, Roco CM, Muscat RA *et al*. Single-cell profiling of the developing mouse brain and spinal cord with split-pool barcoding. *Science* 2018;**360**:176–182.

Rowland DC, Obenhaus HA, Skytøen ER *et al*. Functional properties of stellate cells in medial entorhinal cortex layer II. *Elife* 2018;**7**:e36664.

Sturchler-Pierrat C, Abramowski D, Duke M *et al*. Two amyloid precursor protein transgenic mouse models with Alzheimer disease-like pathology. *Proc Natl Acad Sci USA* 1997;**94**:13287–13292.

Venkataraman AV, Mansur A, Rizzo G *et al*. Widespread cell stress and mitochondrial dysfunction occur in patients with early Alzheimer's disease. *Sci Transl Med* 2022;**14**:eabk1051.

Yao Z, Van Velthoven CT, Nguyen TN *et al*. A taxonomy of transcriptomic cell types across the isocortex and hippocampal formation. *Cell* 2021;**184**:3222–3241. e26.

Yi J, Chen B, Yao X *et al*. Upregulation of the lncRNA MEG3 improves cognitive impairment, alleviates neuronal damage, and inhibits activation of astrocytes in hippocampus tissues in Alzheimer's disease through inactivating the PI3K/Akt signaling pathway. *J Cell Biochem* 2019;**120**:18053–18065.

Yin F, Sancheti H, Patil I *et al*. Energy metabolism and inflammation in brain aging and Alzheimer's disease. *Free Radical Biol Med* 2016;**100**:108–122.

Ying J, Keinath AT, Lavoie R *et al*. Disruption of the grid cell network in a mouse model of early Alzheimer's disease. *Nat Commun* 2022;**13**:886.

Zalocusky KA, Najm R, Taubes AL *et al*. Neuronal ApoE upregulates MHC-I expression to drive selective neurodegeneration in Alzheimer's disease. *Nat Neurosci* 2021;**24**:786–798.

Zhang T, Shen Y, Guo Y *et al*. Identification of key transcriptome biomarkers based on a vital gene module associated with pathological changes in Alzheimer's disease. *Aging (Milano)* 2021;**13**:14940–14967.

Zhang J, Li D, He K *et al*. Aging-induced YTHDF aggregates impair mitochondrial function by trapping mitochondrial RNAs and suppressing their expression in the brain. *Protein Cell* 2024;**15**:149–155.

Zhong S, Wang M, Zhan Y *et al*. Single-nucleus RNA sequencing reveals transcriptional changes of hippocampal neurons in APP23 mouse model of Alzheimer's disease. *Biosci Biotechnol Biochem* 2020;**84**:919–926.

Ziegenhain C, Vieth B, Parekh S *et al*. Comparative analysis of single-cell RNA sequencing methods. *Mol Cell* 2017;**65**:631–643.e4.